Journal of Power Sources 488 (2021) 229454

Contents lists available at ScienceDirect

Journal of Power Sources

journal homepage: www.elsevier.com/locate/jpowsour

Electrochemical impedance spectroscopy study of lithium-ion capacitors: Modeling and capacity fading mechanism

Xiaohu Zhang [a], Xiong Zhang [a,b,d,*], Xianzhong Sun [a,b], Yabin An [a], Shuang Song [a,b], Chen Li [a], Kai Wang [a,b,d], Fangyuan Su [c,d], Cheng-Meng Chen [c,d], Fangyan Liu [d], Zhong-Shuai Wu [d], Yanwei Ma [a,b,e,**]

[a] Institute of Electrical Engineering, Chinese Academy of Sciences, Beijing, 100190, China
[b] School of Engineering Sciences, University of Chinese Academy of Sciences, Beijing, 100049, China
[c] CAS Key Laboratory of Carbon Materials, Institute of Coal Chemistry, Chinese Academy of Sciences, Taiyuan, 030001, Shanxi, China
[d] Dalian National Laboratory for Clean Energy, Chinese Academy of Sciences, Dalian, 116023, China
[e] School of Materials Science and Engineering, Zhengzhou University, Zhengzhou, Henan, 450001, China

HIGHLIGHTS

- The impedance performances of LICs have been analyzed using EIS.
- Impedance equivalent circuit model of LICs is established.
- The impedance characteristics of LICs are analyzed with various *U*ocv and cycle numbers.
- The capacity retention ratio of LICs is 94.5% after 200,000 cycles at 2.2–3.8 V.

ARTICLE INFO

Keywords:
Lithium-ion capacitors
Electrochemical impedance spectroscopy
Equivalent circuit model
Impedance
Cycle numbers

ABSTRACT

As important electrochemical power storage technology, lithium-ion capacitors (LICs) combine the advantages of both electric double layer capacitors (EDLCs) and lithium-ion batteries (LIBs). The impedance performances of LICs have been analyzed using electrochemical impedance spectroscopy (EIS), and the impedance equivalent circuit model (ECM) of LICs is established. Based on the EIS results, the ECM is established to describe the impedance behavior of LICs. The impedance characteristic variations (the ohmic resistance, charge transfer resistance and porous diffusion resistance) of LICs are analyzed with various open circuit voltage and different cycle numbers. The charging-discharging cut-off voltage and the cycle numbers greatly influence the LICs impedance and thus the capacity retention rate. It is shown that the capacity retention ratio is 73.8% after 80,000 cycle numbers when charging-discharging cut-off voltage is set to 2.0–4.0 V. When charging-discharging cut-off voltage is set to 2.2–3.8 V, the capacity retention ratio is 94.5% of the initial value after 200,000 cycle numbers. It provides useful guidance for setting the charging-discharging cut-off voltage of LICs.

1. Introduction

Energy storage technology has gradually become a key supporting technology for smart grids, alternative energy sources to generate electricity and energy [1,2]. In addition, green transportation, such as electric vehicles, hybrid electric vehicles and electric power transportation, is actively carried out all over the world [3,4]. For these reasons, the demand for electrochemical energy storage technology in social development is urgent, and new electrochemical energy storage technology keeps emerging. Electrochemical energy storage technology with long life, high safety, high power density and high energy density is increasingly favored by people [5–10]. Among innovative electrochemical energy storage devices, lithium-ion capacitors (LICs) are receiving huge interest from both industry and academia. LICs are hybrid energy storage systems between electric double layer capacitors (EDLCs) and lithium-ion batteries (LIBs). The positive electrode is

* Corresponding author. Institute of Electrical Engineering, Chinese Academy of Sciences, Beijing, 100190, China.
** Corresponding author. Institute of Electrical Engineering, Chinese Academy of Sciences, Beijing, 100190, China.
E-mail addresses: zhangxiong@mail.iee.ac.cn (X. Zhang), ywma@mail.iee.ac.cn (Y. Ma).

https://doi.org/10.1016/j.jpowsour.2021.229454
Received 1 December 2020; Received in revised form 28 December 2020; Accepted 3 January 2021
Available online 12 January 2021
0378-7753/

activated carbon (AC), and the negative electrode is lithium-ion pre--doped carbon, such as graphite, soft carbon, hard carbon, MXenes film-based electrode, etc. [11–20]. LICs utilize a high-surface area AC as the positive electrode and a lithium-ion doped carbon as the negative electrode, which support the quick and reversible intercalation of lithium ions. During the charge/discharge process, the intercalation/de-intercalation of lithium-ions occurs within the bulk of negative electrode, whereas the adsorption/desorption of anions occurs on the surface of the corresponding AC positive electrode. As a result, the energy density of LICs is 3–5 times higher than that of EDLCs, and the power density can reach up to 30 kW kg^{-1} [21–24].

As in LIBs and EDLCs, the internal resistance of LICs is one of the most important parameters to evaluate their electrochemical performances, and has an important influence on the effective voltage range, reliability, cycle life, and cell consistency [25]. It is also an important technical parameter to accurately judge LICs performance in a timely manner, and it can reflect the internal state of the device. Therefore, it is very important to test and analyze the LICs impedance. Electrochemical impedance spectroscopy (EIS) is a powerful and non-invasive method of measuring the LICs impedance behavior over a wide frequency rang. When using EIS, a properly designed equivalent circuit model (ECM) of LICs is necessary. The data acquired from EIS can be analyzed and used to populate circuit elements in the ECM in parallel with identifying high-level electrochemical phenomena, and it can analyze the internal resistance variation characteristics of LICs by the ECM [26–28]. So, EIS was used by many researchers to identify model parameters and analyze LICs impedance characteristics. Dsoke et al. analyzed the effects of electrodes thicknesses on the power and energy performances of LICs based on AC and $Li_4Ti_5O_{12}$ (LTO) through comparing the EIS profiles of LICs with different capacity ratios of AC and LTO [29]. Naderi et al. proposed a reduced charge transfer and Warburg diffusion resistances to examine the intermittent EIS results based on the potential at which the anode was operating [30]. In order to explain the dynamic behavior of LICs, Barcellona et al. proposed a new electric model, where the parameters of the proposed model were tuned by means of EIS and interpolated to work at any voltage and any temperature [31]. However, LICs are energy storage systems with very long cycle life, and the impedance characteristics with different cycle numbers with real-time and operating conditions are few studied.

This work focuses on the LIC cells prepared in our research group. The impedance performances of LICs were analyzed using EIS, and the LICs impedance ECM was established. We further examined these factors influencing the characteristic parameters. The present study provides a theoretical foundation for the commercial application of LICs prepared in the research group. The LICs impedance increases greatly and capacity decays faster when charging-discharging cut-off voltage is set to 2.0–4.0 V. While charging-discharging cut-off voltage is set to 2.2–3.8 V, LICs have a long cycle aging, of course with the decrease of energy density.

2. Experimental

2.1. Preparation of LICs

The LICs used in this study adopted a laminated structure. In the LICs pilot line of our research group, we produced 900F soft-packed LICs. Fig. 1 (a) shows a schematic view of the LICs. The device is formed by stacking positive electrode, separator, and negative electrode. Positive and negative electrodes laminate, containing porous current collectors, which are placed and separated alternately by separator panels. Lithium

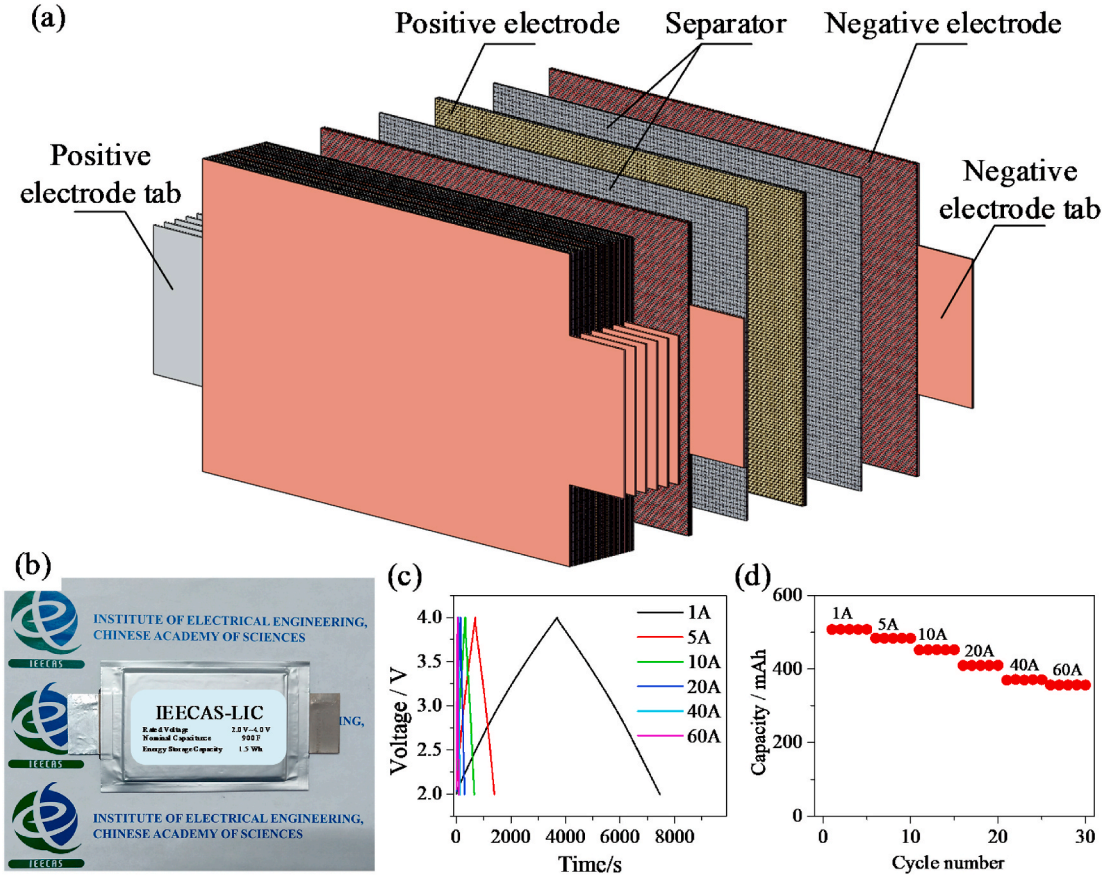

Fig. 1. Preparation of LICs: (a) LIC schematic view, (b) photo of LIC cell, (c) LIC charge-discharge curves at different currents, and (d) LIC discharge capacity at different currents.

foil is adjacent to the anode and is directly connected through the copper tabs. The device with this configuration exhibits excellent electrochemical performance and a good current charge-discharge capability. Fig. 1 (b) shows the LICs cell picture and the relevant parameters, Fig. 1 (c) and Fig. 1 (d) show the charging-discharging voltage and capacity curves of LICs at different currents, respectively. The nominal capacitance is tested to be 900 F using 1 A current at 25 °C. The stored energy is 1.5 Wh and capacity is 500 mA h. Due to polarization, the capacity of LICs decreases gradually with the increase of charge/discharge current. When the charge-discharge current is 10 A, the capacity is 450 mA h. The technical parameters of IEECAS-LIC900F are listed in Table 1.

2.2. Experimental platform and setup

The LICs experimental platform consists of the 5 V/60 A charge-discharge test system (NEWARE, Shenzhen, China), high-low temperature incubator, electrochemical workstation (Metrohm, Switzerland), and personal computer.

The EIS was measured using the electrochemical workstation. The impedance spectra of LIC were recorded in the frequency range from 10 mHz to 1 kHz at the amplitude of AC signal of 10 mV. NOVA software was used for the ECM fitting. The test of impedance cycling characteristics was performed in several steps: a) constant current charge at 10 A and a cut-off voltage of 4.0 V; b) constant current discharge at 10 A and a cut-off voltage of 2.0 V; c) steps a) and b) repeated for 20,000 cycle numbers; d) test the EIS of LICs with various open-circuit voltages (2.0–4.0 V) at room temperature (25 ± 1 °C); e) steps a) and d) repeated 4 cycle numbers.

The voltage between positive and negative electrodes is an open-circuit voltage (U_{OCV}) during the EIS investigation of LICs. This assumption was made because the LICs was positioned in the EIS test for a long time, and the current that passed through the LICs during the test was minimal. This process exists without polarization voltage. Besides, there is a linear relationship between the U_{OCV} and a state-of-charge (*SOC*) [32,33]. Therefore, impedance spectra recorded with different values of U_{OCV} correspond to different *SOC*.

3. Electrochemical impedance model of LICs

The basic functional components of LICs include positive and negative current collector, electrode material, electrolyte and separator. During operation, anions and cations of the electrolyte undergo different processes. At the negative electrode, insertion and extraction of lithium ions take place. At the same time, absorption and desorption of ions (Li^+ and PF_6^-) happen at the positive electrode. In Fig. 2 (a), the impedance distribution of LICs mainly can be divided into three parts, in general [34,35].

(1) The ohmic impedance: it mainly includes the contact resistance that associates with the electrical contact between active materials and the current collector, and associates with ionic conduction in the electrolyte phase and electronic conduction in the electrode phase [36].
(2) The interfacial impedance: it mainly includes the charge transfer impedance and the diffusion impedance of SEI film [37]. The charge transfer impedance associates with charge transport of Li^+ and LiF_6^- through the charge transfer reactions therein. The diffusion impedance of SEI film associates with charge transport of Li^+ and LiF_6^- through the SEI film [38,39].
(3) Diffusion impedance of the porous electrode: it mainly includes the dynamic characteristics of the porous electrode material and the diffusion impedance of Li^+ and LiF_6^- on the pore electrolyte of the porous electrode [40,41].

Table 1
Technical parameters of IEECAS-LIC900F.

SPECIFICATIONS	IEECAS-LIC900F
Rated Voltage	2.0–4.0 V
Nominal Capacitance	900 F
Stored Energy	1.5 Wh
Energy Density	22 Wh/kg
Weight	68 g
Dimension	84 × 135 × 5 mm (L × W × H)

The impedance characteristics of LICs were analyzed by EIS at U_{OCV} of 3.4 V. Fig. 2 (b) shows the impedance spectrum from high (left) to low (right) frequencies. The impedance spectrum shows an almost regular semicircle and two oblique lines with different slopes in the first quadrant. A straight line can be seen in the fourth quadrant, being characteristic for inductance (L) which is mainly the effect of electrode roughness.

As the frequency decreases, the impedance curve extends from the fourth to the first quadrant, intersecting the real part of the impedance at the internal ohmic resistance (R_o). This can be defined as the distance of the first half-circle point from the Y-axis [42]. In the intermediate frequency range (17 Hz ~ 600 Hz), the semicircle in the Nyquist plot represents the charge transfer between electrolyte and electrode. This process is slower and occurs in the time range from 1.67 to 58.8 ms. The physical interpretation of this process corresponds to the embedment/ejection of internal LIC ions and ion adsorption/desorption, which is represented as a parallel combination of R_{ct} and C_{dl} in the equivalent circuit [43]. R_{ct} is the charge transfer resistance or electrochemical reaction resistance, and C_{dl} is the electrical double-layer capacitance. The low-frequency band (10 mHz–17 Hz) reflects the diffusion process of Li^+ and PF_6^- in the porous electrode. In Fig. 2 (a), the impedance spectrum depicts a Warburg impedance line close to 45° slope (115 mHz −17 Hz) and a low-frequency impedance line close to the vertical slope (10–115 mHz), which together constitute the LICs diffusion impedance or concentration polarization resistance. The Warburg diffusion behavior observed in the low-frequency range of the impedance spectra can be represented by the transmission line model (TLM-PSD) proposed by Levi et al. [44,45]. The model consists of the finite-length-Warburg (FLW) element of the cell in series with intercalation capacitance (C_W). A standard Warburg impedance Z_W is a special case of the constant phase element (CPE), occurring when the angle in the Nyquist plot is equal to 45°. However, the obtained EIS data exhibits a slope higher than 45°. This may be explained by ion diffusion in the electrodes in a spherical structure, but not along only one direction. Therefore, the Warburg impedance Z_W is replaced by CPE (Q_W). The admittance, impedance, and constant phase angle element are shown in equation (1). The admittance is defined as the inverse electrical impedance, Zw:

$$\frac{1}{Z_W} = Y_W = Q_W^0 \cdot (j\omega)^n \quad (1)$$

where Y_W is admittance, Q_W^0 is numerically equal to admittance at ω = 1 rad/s refers to the unit [$S \cdot s^n$], and n is the slope of the semi-line from 0 to 1. For $n = 1$, it represents a capacitor, and for $n = 0$, it represents a resistor. The angle ϕ between the low-frequency impedance line is close to the vertical slope and the real axis is approximately 82.5°. The slight deviation from the ideal vertical line can be interpreted as the consequence of the pore size distribution of porous materials. At low frequencies, the impedance becomes purely capacitive, because the ions can no longer diffuse into the material, so the capacity is formed by the ions surrounding the electrode material [46]. Therefore, the low-frequency impedance close to the vertical slope is modeled by the capacitive element C_W. For the development of the equivalent circuit model, the equivalent elements are connected in parallel for the simultaneous steps and in series for the successive steps. The impedance model is shown in Fig. 2 (d). To verify the accuracy of the impedance model, we calculated the parameters of the impedance model using

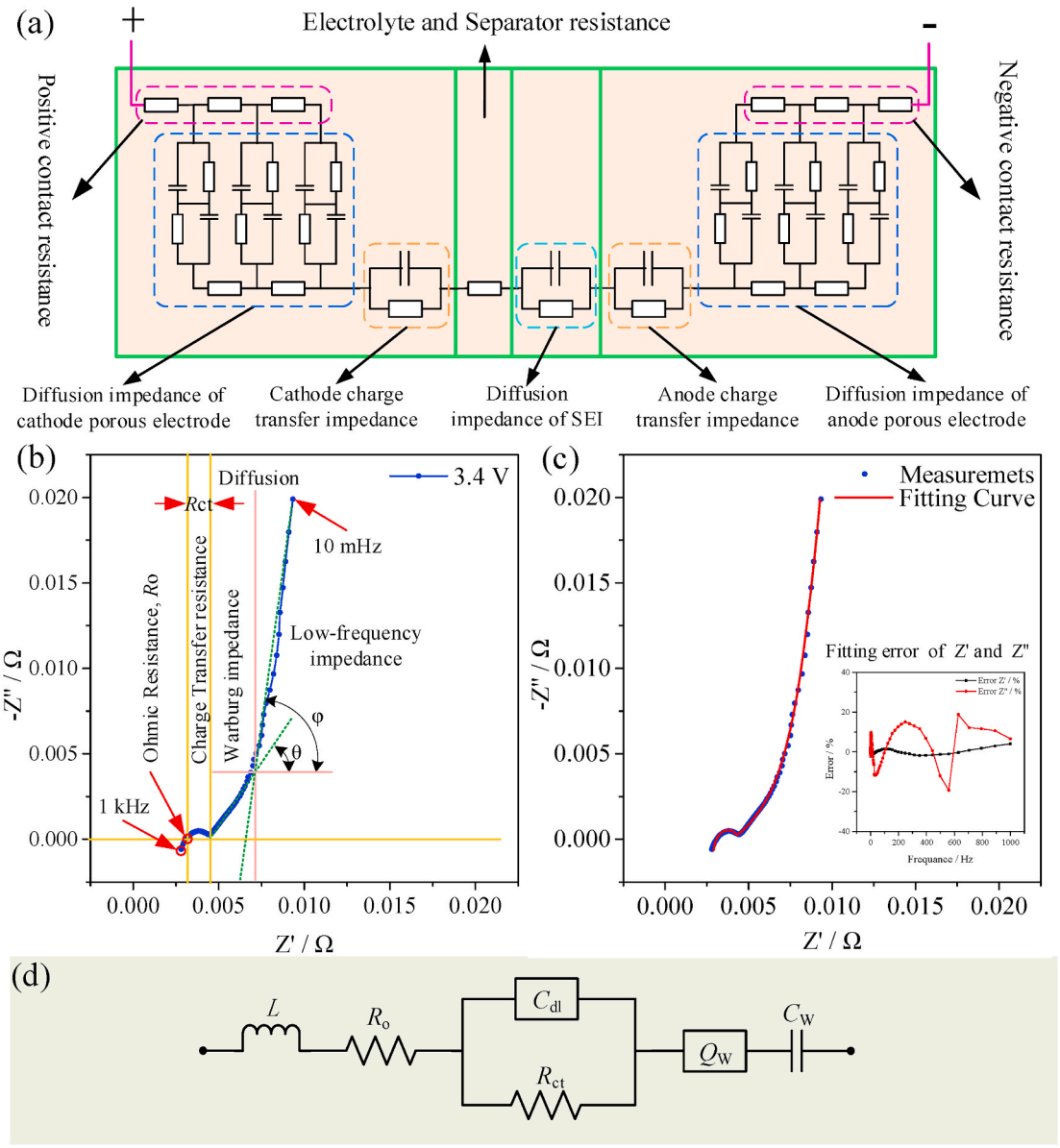

Fig. 2. (a) Impedance distribution of LICs, (b) the EIS of LIC at 3.4 V, (c) the fitting result and fitting error (inset), and (d) the impedance model used to fit the EIS.

different parameter values. The impedance values at different frequency points are calculated and compared with the measured impedance data. The fitting result of the electrochemical impedance model is shown in Fig. 2 (c) and the fitting parameters are listed in Table 2. We can see that the curves are measured and fitted in good agreement. The comparison and error analysis of the experimental and fitted data shows that the discrepancy between these two datasets is within 2%.

Table 2
The parameters of the impedance model.

Number	Parameter	Value	Description
1	L/H	1.619×10^{-7}	Pure inductor
2	R_o/Ω	0.003076	Ohmic resistance
3	R_{ct}/Ω	0.002492	Charge transfer resistance
4	C_{dl}/F	0.4203	Pure capacitance
6	Y_W/S· s^n	404.9	Admittance
7	n_W	0.3586	Dimensionless exponents
8	C_W/F	985.4	Pure capacitance

4. Results and discussion

4.1. EIS characteristics of LICs with various open-circuit voltages

LICs like other energy storage systems, show different behavior at different frequency ranges. Fig. 3 shows impedance spectra obtained at various U_{OCV} from 2.0 to 4.0 V. The left part of the arc lays closer to the x-axis direction, while the right part is more dispersed. The height of the arc varies significantly with U_{OCV}, where the ohmic resistance R_o does not change substantially with U_{OCV}. However, the charge transfer resistance R_{ct} exhibits a significant variation with U_{OCV}. Besides, the straight lines that represent concentration polarization at various voltages are almost parallel, and the effect of U_{OCV} on the concentration polarization cannot be determined from the available data.

To analyze further the effect of U_{OCV} on the shape of impedance spectra, we analyzed the parameters of the ECM represented by different frequency bands of the impedance spectra. The main conclusions are given as follows. As shown Fig. 4, the R_o and R_{ct} gradually decreases in the range of U_{OCV} from 2.0 to 3.4 V and gradually increases from 3.4 to 4.0 V, and the Y_W is going in the opposite direction. With the continuous

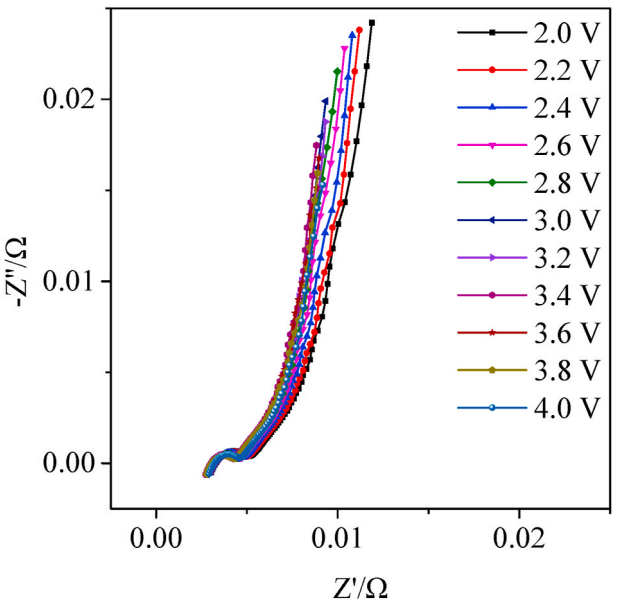

Fig. 3. Nyquist plots obtained at various U_{OCV}.

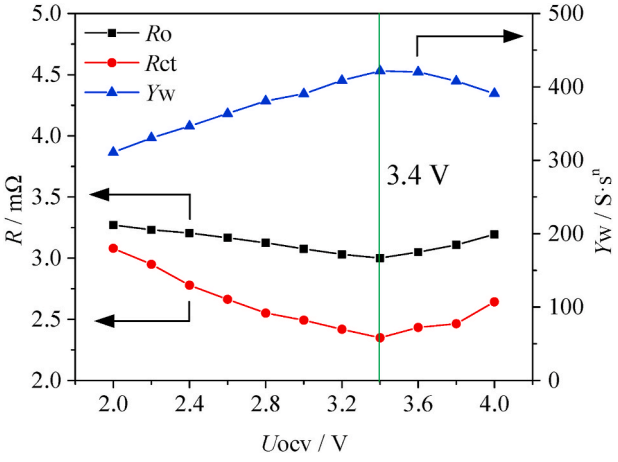

Fig. 4. Ohmic resistance R_o, charge transfer resistance R_{ct}, and Warburg impedance admittance Y_W at various U_{OCV}.

increase of U_{OCV}, the volume expansion of positive and negative electrodes yields a shorter distance between separator and solution. At the same time, the concentration of ions in solution decreases. Volume expansion will lead to impedance reduction, while ion concentration reduction will lead to impedance increase. In the case of 2.0–3.4 V, the degree of impedance reduction is greater than that of impedance increase; however, in the case of 3.4–4.0 V, the degree of impedance reduction is smaller than that of impedance increase. Since the electrochemical polarization is related to the polarization voltage in the charging-discharging process, the U_{OCV} should be selected carefully in the view of the LICs service life. At the same time, the attention should be paid to overvoltage and undervoltage protection during charging in the high U_{OCV} range and discharging in the low U_{OCV} range to prevent the LICs damage.

4.2. LICs resistance characteristics with different cycle numbers

The LIC was tested at the charging-discharging current of 10 A for 80,000 cycle numbers and the relationship between discharge capacity is shown in Fig. 5. As shown in Fig. 5 (a), the capacity retention ratio is 73.8% of the initial value after 80,000 cycle numbers. According to the

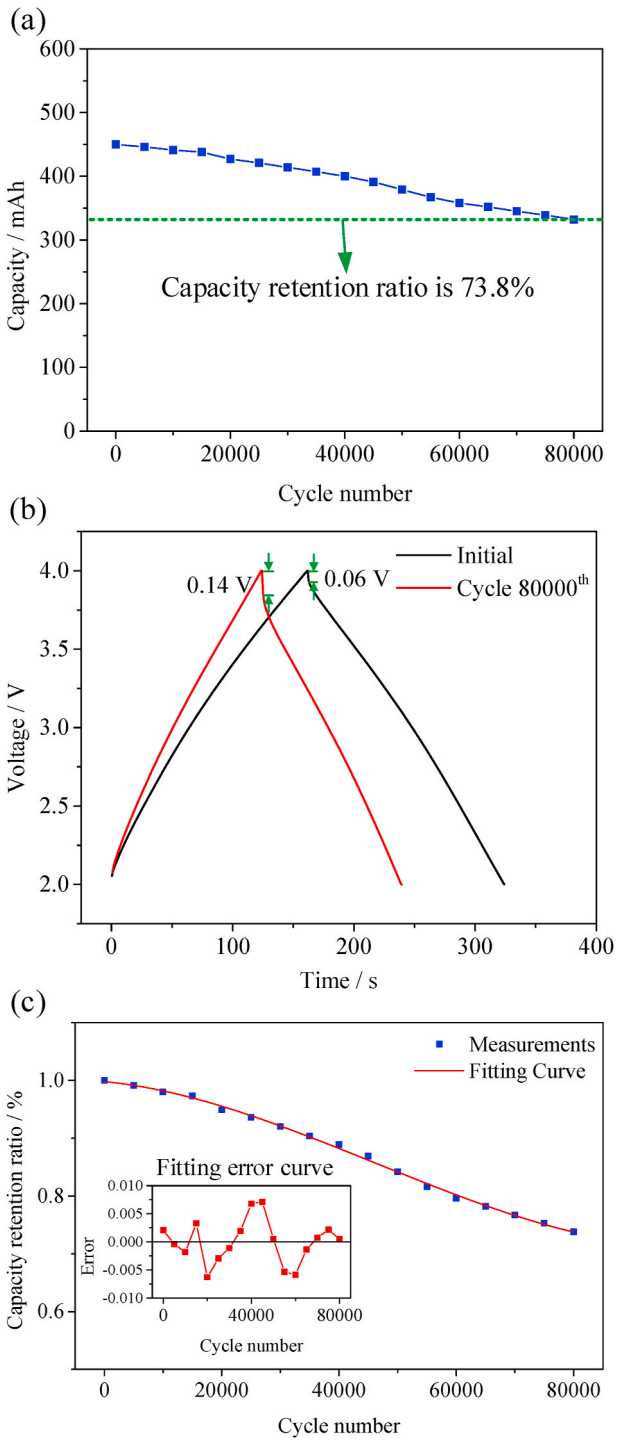

Fig. 5. (a) LICs discharge capacity with different cycle numbers, (b) LICs charge-discharge voltage curves with the initial and 80,000th cycle, and (c) LICs capacity retention ratio with different cycle numbers and simulation fitting curve.

charging-discharging curve, the LIC charging-discharging time decreases, and the polarization increases. As shown in Fig. 5 (b), when the LICs is charge to discharge conversion, the polarization voltage of the initial cycle is 0.06 V and increases to 0.14 V after 80,000 cycle numbers.

The capacity retention ratio at different cycling numbers and the simulation curve are also given as shown in Fig. 5 (c). Using the Matlab Curve Fitting module, the capacity retention rate is fitted to obtain the relationship between the LICs capacity retention rate and the cycle

numbers:

$$m = 4.84 \times 10^{-16} \cdot N^3 - 6.71 \times 10^{-11} \cdot N^2 - 9.81 \times 10^{-7} \cdot N + 0.998 \quad (2)$$

Where m is the capacity retention rate, and N is cycle number. The discrepancy between the measured data and the fitting model is within 1%.

With the increasing of the cycle numbers, the surface is partly covered with electrolyte decomposition products, which induces the decline of the LICs capacity. Of course, the change in anode potential will affect the kinetics of the anode, which will affect the overall LICs impedance. Then, with the increasing of the cycle numbers, SEI formation and growth leads to an impedance rise at the anode. These mechanisms initiate the decrease of the overall capacitance and the increase of the resistance. Furthermore, electrode cracks may result afterward. Solid products of these reactions may deposit on the surface of activated carbon and block the pores, which can affect the microstructure of the electrodes due to the consequent change of pore size [47,48].

Fig. 6 presents the impedance spectra of LICs after different cycle numbers at the U_{OCV} values of 2.0 V, 3.4 V, and 4.0 V, respectively. The ohmic resistance R_o does not alter substantially different with the increase of cycle numbers. However, the semicircle enlarges with the cycle numbers at the cost of the straight tail at the low-frequency side. This shows that Faradaic impedance increases, while the interfacial charge transfer reaction decelerates. The state of charge also affects the shape and amplitude of the impedance [49]. The increase of the semicircle corresponds to the substantial rise of the charge transfer resistance R_{ct}, especially after 40,000 cycle numbers. With the rise of the cycle numbers, the radius of the capacitance-reactance arc increases, and the diffusion part of the impedance spectrum notably changes. This phenomenon is especially apparent at low and high U_{OCV} values.

The ohmic resistance R_o directly affects the power characteristics, energy efficiency, and thermal behaviors of LICs. Besides, it can also be used to assess whether the LICs is failure. At a low cycle number, R_o does not substantially change with U_{OCV}. However, with the increase of cycle number, R_o increases, especially at high U_{OCV} values. Fig. 7 (a) and Fig. 7 (b) show the variation trend and the cumulative growth rate of LICs ohmic resistance R_o with different cycle numbers, respectively. The ohmic resistance R_o changes slightly in the U_{OCV} range from 2.0 to 3.6 V, but it increases at 3.6–3.8 V with the increase of the cycle number. The cumulative growth rate of ohmic resistance R_o is 36% after 80,000 cycle numbers at 4.0 V. This is mainly caused by the decomposition of electrolyte, as described in Ref. [50]. The charging-discharging cut-off voltage can be appropriately reduced according to the ohmic resistance variation. The LICs cut-off voltage should be reduced especially in the high voltage area to ensure long service life. As a trade-off, it will reduce the energy density.

The charge transfer resistance R_{ct} reflects the attenuation degree of the LICs, which gradually increases with charging-discharging cycle numbers. The variation trend and cumulative growth rate of R_{ct} with different cycle numbers are shown in Fig. 7 (c), respectively. The charge transfer resistance R_{ct} in high and low U_{OCV} ranges increases rapidly after 40,000 cycle numbers. The charge transfer resistance R_{ct} shows an overall growth trend with increasing of the cycle numbers. In the low U_{OCV} range, from 2.0 to 2.4 V, the charge transfer resistance R_{ct} changes substantially. As shown in Fig. 7 (d), in the first 40,000 cycle numbers, the slope of the R_{ct} growth rate is the same, but after 40,000 cycle numbers, R_{ct} increases significantly, exhibiting a high slope. According to the above analysis, the change of R_{ct} during the cycling process mainly comes from two aspects: polarization characteristics in the low U_{OCV} range and the side effects caused by the increase in the cycle number. The R_{ct} increase may originate from the formation of SEI layer at the electrode-electrolyte interface, which restricts the lithium-ion migration pathway, and hinders the transport of lithium ions through the electrode-electrolyte interface [51,52].

The porous diffusion resistance Y_W, reveals the dynamic properties of porous electrode materials and the diffusion impedance of ions in pores. It plays a vital role in the optimization of LICs energy density and maximum power density. As shown in Fig. 7 (e) and Fig. 7 (f), Y_W increases with the increasing of the cycle numbers, especially when U_{OCV} is 4.0 V. The diffusion coefficients in both electrolyte and solid-phase decrease remarkably with aging. Moreover, the electrolyte phase diffusion dominates over the solid-phase diffusion in the low-frequency diffusion impedance, and the aging-induced increase in the diffusion impedance is mainly caused by the electrolyte-phase diffusion [53].

Therefore, when the LICs is used, it is not suggested to use high current charge-discharge in the voltage interval between the two ends, so it is necessary to control the charge-discharge cut-off voltage properly, and to carry out overvoltage protection and undervoltage protection to avoid damage to LICs. As shown in Fig. 8, the cycle life test when the cut-off voltage of charge and discharge is 2.2–3.8 V. The capacity retention ratio is 94.5% of the initial value after 200,000 cycle numbers. The capacity decrease during the cycling is mainly due to the SEI layer growth at the negative surface, which causes the increase in the LICs resistance increase and slow-down of the charge transfer and diffusion processes in anode electrode [54]. It can also be concluded that the capacity decay and cycle life of the LICs is mainly limited by the negative electrode. The resistance increase can also be used to explain the decrease of capacity.

5. Conclusion

EIS measurements and capacity tests, as well as other performance experiments of LICs, were performed at different cycle stages. Based on the EIS results, the ECM was established to describe the LICs impedance behavior. The ohmic resistance, charge transfer resistance, and diffusion impedance were determined. This approach shows good potential to indicate capacity degradation behavior. LICs cycle aging, the increase of cell impedance, and capacity decay were originated from multiple and

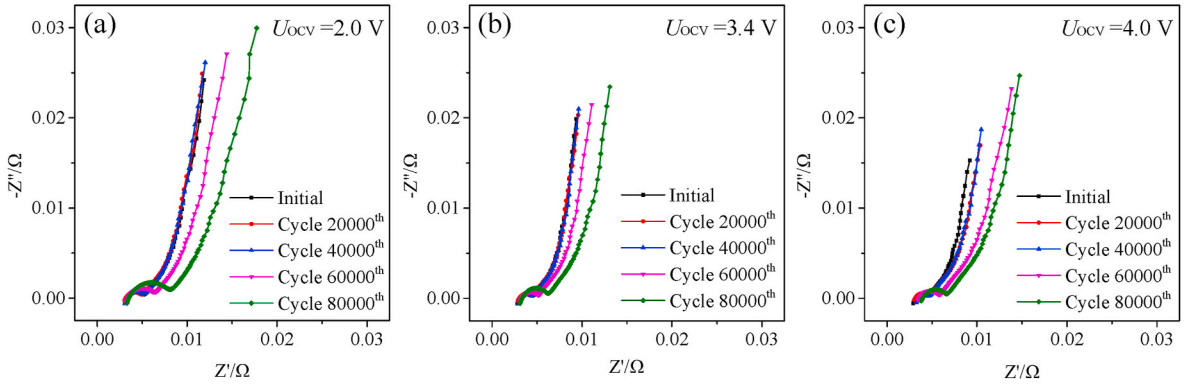

Fig. 6. Impedance spectra of LICs after different cycle numbers at various U_{OCV}: (a) 2.0 V, (b) 3.4 V, and (c) 4.0 V.

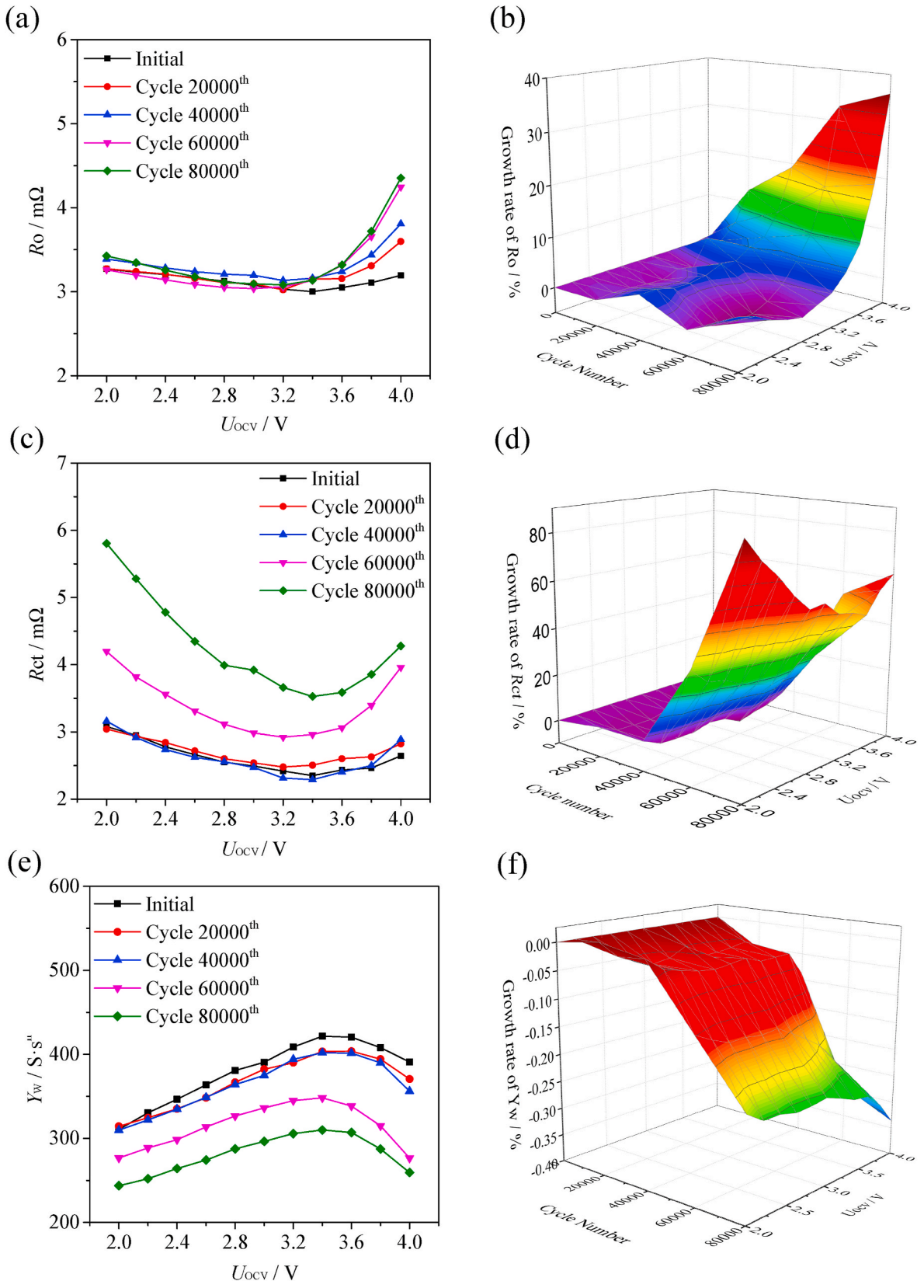

Fig. 7. (a) R_o and (b) the R_o growth rate of at different cycle numbers and various U_{OCV}; (c) R_{ct} and (d) the R_{ct} growth rate with different cycle numbers and various U_{OCV}; (e) *Y*w and (f) the *Y*w growth rate with different cycle numbers and various U_{OCV}.

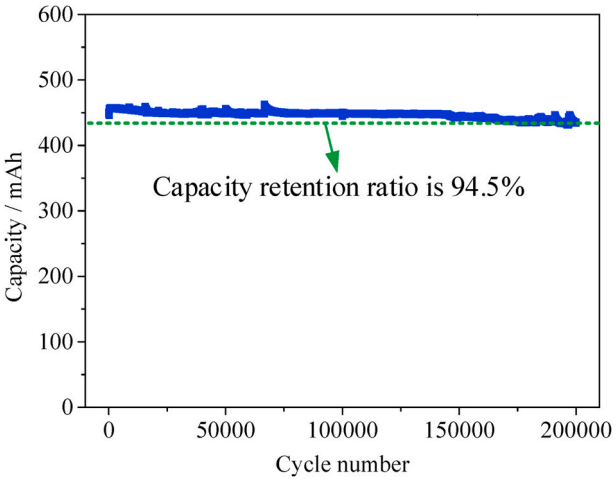

Fig. 8. LICs discharge capacity with 200,000 cycle numbers.

complex mechanisms. Depending on the LICs structure, both high and low U_{OCV} (i.e., state-of-charge) may deteriorate performance and shorten the LICs service life. It is necessary to control the charging-discharging cut-off voltage properly and to provide overvoltage and undervoltage protection. With the increase of cycle aging, LICs internal resistance increases, and the difference of internal resistance with various U_{OCV} increases. Therefore, according to the capacity requirements for an appropriate application, the power and cycle aging determine the LICs charging-discharging cut-off voltage. Remarkably, the LICs charging-discharging cut-off voltage is set to 2.0–4.0 V when high capacity is required, while it is set to 2.2–3.8 V when more extended cycle life is required. To extend the service life, and reduce the cycle costs, a gradient utilization can be implemented, i.e., LICs can be applied in a low-power range after the high-power application is exhausted. The next step is to compare and analyze the evolution relation between cycle life, capacity, and internal resistance under conditions of different ratios and temperatures. Based on this, the LICs life model will be established.

CRediT authorship contribution statement

Xiaohu Zhang: Data curation, Methodology, Writing - original draft, Writing - review & editing. **Xiong Zhang:** Conceptualization, Supervision, Funding acquisition, Writing - review & editing. **Xianzhong Sun:** Writing - review & editing. **Yabin An:** Writing - review & editing. **Shuang Song:** Writing - review & editing. **Chen Li:** Writing - review & editing. **Kai Wang:** Writing - review & editing. **Fangyuan Su:** Writing - review & editing. **Cheng-Meng Chen:** Writing - review & editing. **Fangyan Liu:** Writing - review & editing. **Zhong-Shuai Wu:** Writing - review & editing. **Yanwei Ma:** Supervision, Project administration, Writing - review & editing.

Declaration of competing interest

The authors declare that they have no known competing financial interests or personal relationships that could have appeared to influence the work reported in this paper.

Acknowledgements

This work was financially supported by the National Natural Science Foundation of China (Nos. 52077207, 51822706, 51777200), Beijing Natural Science Fundation (JQ19012), the Strategic Priority Research Program of Chinese Academy of Sciences (No. XDA21050302), the Dalian National Laboratory for Clean Energy Cooperation Fund, the CAS (Nos. DNL201912, DNL201915).

References

[1] S. Chu, A. Majumdar, Opportunities and challenges for a sustainable energy future, Nature 488 (2012) 294–303.
[2] K.K. Zame, C.A. Brehm, A.T. Nitica, C.L. Richard, G.D. Schweitzer III, Smart grid and energy storage: policy recommendations, Renew. Sustain. Energy Rev. 82 (2018) 1646–1654.
[3] S.S. Williamson, A.K. Rathore, F. Musavi, Industrial Electronics for electric transportation: current state-of-the-art and future challenges, IEEE Trans. Ind. Electron. 62 (2015) 3021–3032.
[4] B.Q. Guo, M. Niu, X.K. Lai, L.Q. Chen, Application research on large-scale battery energy storage system under Global Energy Interconnection framework, Global Energy Interconnection 1 (2018) 79–86.
[5] D. Larcher, J.M. Tarascon, Towards greener and more sustainable batteries for electrical energy storage, Nat. Chem. 7 (2015) 19–29.
[6] M. Bandhauer, S. Garimella, T.F. Fuller, A critical review of thermal issues in lithium-ion batteries, J. Electrochem. Soc. 158 (2011) R1–R25.
[7] D. Yan, L. Lu, Z. Li, X. Feng, M. Ouyang, F. Jiang, Durability comparison of four different types of high-power batteries in HEV and their degradation mechanism analysis, Appl. Energy 179 (2016) 1123–1130.
[8] N.L. Wulan Septiani, Y.V. Kaneti, K.B. Fathoni, J. Wang, Y. Ide, B. Yuliarto, Nugraha, H.K. Dipojono, A.K. Nanjundan, D. Golberg, Y. Bando, Y. Yamauchi, Self-assembly of nickel phosphate-based nanotubes into two-dimensional crumpled sheet-like architectures for high-performance asymmetric supercapacitors, Nano Energy 67 (2020) 104270.
[9] Y. Li, J. Henzie, T. Park, J. Wang, C. Young, H. Xie, J.W. Yi, J. Li, M. Kim, J. Kim, Y. Yamauchi, J. Na, Fabrication of flexible microsupercapacitors with binder-free ZIF8 derived carbon films via electrophoretic deposition, Bull. Chem. Soc. Jpn. 93 (2020) 176–181.
[10] S.R. Sivakkumar, A.G. Pandolfo, Evaluation of lithium-ion capacitors assembled with prelithiated graphite anode and activated carbon cathode, Electrochim. Acta 65 (2012) 280–287.
[11] J.M. Campillo-Robles, X. Artetxe, K. del Teso Sánchez, C. Gutiérrez, H. Macicior, S. Röser, R. Wagner, M. Winter, General hybrid asymmetric capacitor model: validation with a commercial lithium ion capacitor, J. Power Sources 425 (2019) 110–120.
[12] X.Z. Sun, X. Zhang, W.J. Liu, K. Wang, C. Li, Z. Li, Y.W. Ma, Electrochemical performances and capacity fading behaviors of activated carbon/hard carbon lithium ion capacitor, Electrochim. Acta 235 (2017) 158–166.
[13] C. Li, X. Zhang, K. Wang, X. Sun, Y. Ma, High-power lithium-ion hybrid supercapacitor enabled by holey carbon nanolayers with targeted porosity, J. Power Sources 400 (2018) 468–477.
[14] P.X. Han, G.J. Xu, X.Q. Han, J.W. Zhao, X.H. Zhou, G.L. Cui, Lithium ion capacitors in organic electrolyte system: scientific problems, material development, and key technologies, Adv. Energy Mater. 8 (2018) 1801243.
[15] N. Hirota, K. Okuno, M. Majima, A. Hosoe, S. Uchida, M. Ishikawa, High-performance lithium-ion capacitor composed of electrodes with porous three-dimensional current collector and bis (fluorosulfonyl) imide-based ionic liquid electrolyte, Electrochim. Acta 276 (2018) 125–133.
[16] A. Shellikeri, S. Yturriaga, J.S. Zheng, W. Cao, M. Hagen, J.A. Read, T.R. Jow, J. P. Zheng, Hybrid lithium-ion capacitor with $LiFePO_4$/AC composite cathode-Long term cycle life study, rate effect and charge sharing analysis, J. Power Sources 392 (2018) 285–295.
[17] J.S. Zheng, L. Zhang, A. Shellikeri, W. Cao, Q. Wu, J.P. Zheng, A hybrid electrochemical device based on a synergetic inner combination of Li ion battery and Li ion capacitor for energy storage, Sci. Rep. 7 (2017) 41910.
[18] M. Hagen, W.J. Cao, A. Shellikeri, D. Adams, X.J. Chen, W. Brandt, S.R. Yturriaga, Q. Wu, J.A. Read, T.R. Jow, J.P. Zheng, Improving the specific energy of Li-Ion capacitor laminate cell using hybrid activated Carbon/$LiNi_{0.5}Co_{0.2}Mn_{0.3}O_2$ as positive electrodes, J. Power Sources 379 (2018) 212–218.
[19] P. Zhang, Q.Z. Zhu, R.A. Soomro, S.Y. He, N. Sun, N. Qiao, B. Xu, In situ ice template Approach to fabricate 3D flexible MXene film-based electrode for high performance supercapacitors, Adv. Funct. Mater. 30 (2020) 2000922.
[20] Q.Z. Zhu, J.P. Li, R. Simon, B. Xu, Two-dimensional MXenes for electrochemical capacitor applications: progress, challenges and perspective, Energy Storage Mater. 35 (2021) 630–660.
[21] L. Jin, J.S. Zheng, W. Qiang, A. Shellikeri, S. Yturriaga, R. Gong, J. Huang, J. P. Zheng, Exploiting a hybrid lithium ion power source with a high energy density over 30 Wh/kg, Mater. Today Energy 7 (2018) 51–57.
[22] C. Li, X. Zhang, K. Wang, X.Z. Sun, Y.W. Ma, A 29.3 Wh kg^{-1} and 6 kW kg^{-1} pouch-type lithium-ion capacitor based on SiO_x/graphite composite anode, J. Power Sources 414 (2019) 293–301.
[23] Y.B. An, S. Chen, M. Zou, L.B. Geng, X.Z. Sun, X. Zhang, K. Wang, Y.W. Ma, Improving anode performances of lithium-ion capacitors employing carbon–Si composites, Rare Met. 38 (2019) 1113–1123.
[24] Y.Q. Dai, G.C. Li, X.H. Hai, H.J. Guo, Z.X. Wang, G.C. Yan, J.X. Wang, Ultrathin porous graphitic carbon nanosheets activated by alkali metal salts for high power density lithium-ion capacitors, Rare Met. 39 (2020) 1364–1373.
[25] M. Soltani, J. Ronsmansc, J.V. Mierlo, Cycle life and calendar life model for lithium-ion capacitor technology in a wide temperature range, J. Energy Storage 31 (2020) 101659.
[26] S. Skoog, S. David, Parameterization of linear equivalent circuit models over wide temperature and SOC spans for automotive lithium-ion cells using electrochemical impedance spectroscopy, J. Energy Storage 14 (2017) 39–48.

[27] P. Vyroubal, T. Kazda, Equivalent circuit model parameters extraction for lithium ion batteries using electrochemical impedance spectroscopy, J. Energy Storage 15 (2018) 23–31.
[28] C. Li, L. Gu, X. Guo, D. Samuelis, K. Tang, J. Maier, Charge carrier accumulation in lithium fluoride thin films due to Li-ion absorption by titania (100) subsurface, Nano Lett. 12 (2012) 1241–1246.
[29] S. Dsoke, B. Fuchs, E. Gucciardi, M. Wohlfahrt-Mehrens, The importance of the electrode mass ratio in a Li-ion capacitor based on activated carbon and $Li_4Ti_5O_{12}$, J. Power Sources 282 (2015) 385–393.
[30] R. Naderi, A. Shellikeri, M. Hagen, W. Cao, J.P. Zheng, The influence of anode/cathode capacity ratio on cycle life and potential variations of lithium-ion capacitors, J. Electrochem. Soc. 166 (2019) A2610–A2617.
[31] S. Barcellona, L. Piegari, A lithium-ion capacitor model working on a wide temperature range, J. Power Sources 342 (2017) 241–251.
[32] H. Yang, X.Z. Sun, Y.B. An, X. Zhang, T.Z. Wei, Y.W. Ma, Online parameters identification and state of charge estimation for lithiumion capacitor based on improved Cubature Kalman filter, J. Energy Storage 24 (2019) 100810.
[33] Y.S. Zhang, Z.E. Liu, X.Z. Sun, Y.B. An, X. Zhang, K. Wang, C.H. Dong, Q.H. Huo, T. Z. Wei, Y.W. Ma, Experimental study of thermal charge–discharge behaviors of pouch lithium-ion capacitors, J. Energy Storage 25 (2019) 100902.
[34] A. Nyman, T.G. Zavalis, R. Elger, M. Behm, G. Lindbergh, Analysis of the polarization in a Li-ion battery cell by numerical simulations, J. Electrochem. Soc. 157 (2010) A1236–A1246.
[35] M. Gaberscek, J. Moskon, B. Erjavec, R. Dominko, J. Jamnik, The importance of interphase contacts in Li ion electrodes: the meaning of the high-frequency impedance arc, Electrochem. Solid State Lett. 11 (2008) A170–A174.
[36] H. Blanke, O. Bohlen, S. Buller, R.W. De Doncker, B. Fricke, A. Hammouche, D. Linzen, M. Thele, D.U. Sauer, Impedance measurements on lead–acid batteries for state-of-charge, state-of-health and cranking capability prognosis in electric and hybrid electric vehicles, J. Power Sources 144 (2005) 418–425.
[37] S.E. Li, B.J. Wang, H. Peng, X.S. Hu, An electrochemistry-based impedance model for lithium-ion batteries, J. Power Sources 258 (2014) 9–18.
[38] S.A. Delp, O. Borodin, M. Olguin, C.G. Eisner, J.L. Allen, T.R. Jow, Importance of reduction and oxidation stability of high voltage electrolytes and additives, Electrochim. Acta 209 (2016) 485–510.
[39] A.M. Haregewoin, A.S. Wotango, B.J. Hwang, Electrolyte additives for lithium ion battery electrodes: progress and perspectives, Energy Environ. Sci. 9 (2016) 1955–1988.
[40] W. Cao, J. Zheng, The effect of cathode and anode potentials on the cycling performance of Li-Ion capacitors, J. Electrochem. Soc. 160 (2013) A1572–A1576.
[41] D.G. Moye, P.L. Moss, X.J. Chen, W.J. Cao, S.Y. Foo, A design-based predictive model for lithium-ion capacitors, J. Power Sources 435 (2019) 226694.
[42] R. de Levie, Electrochemical response of porous and rough electrodes, in: P. Delahay (Ed.), Adv. Electrochem. Electrochem. Eng., Interscience, New York, 1967, pp. 329–397.
[43] H.K. Song, Y.H. Jung, K.H. Lee, L.H. Dao, Electrochemical impedance spectroscopy of porous electrodes: the effect of pore size distribution, Electrochim. Acta 44 (1999) 3513–3519.
[44] P.L. Moss, J.P. Zheng, G. Au, P.J. Cygan, E.J. Plichtab, Transmission line model for describing power performance of electrochemical capacitors, J. Electrochem. Soc. 154 (2007) A1020–A1025.
[45] P. Vyroubal, T. Kazda, Equivalent circuit model parameters extraction for lithium ion batteries using electrochemical impedance spectroscopy, J. Energy Storage 15 (2018) 23–31.
[46] C. Fleischer, W. Waag, H.M. Heyn, D.U. Sauer, On-line adaptive battery impedance parameter and state estimation considering physical principles in reduced order equivalent circuit battery models. Part 2. Parameter and state estimation, J. Power Sources 262 (2014) 457–482.
[47] M. Uno, A. Kukita, Cycle life evaluation based on accelerated aging testing for lithium-ion capacitors as alternative to rechargeable batteries, IEEE Trans. Ind. Electron. 63 (2016) 1607–1617.
[48] Y.H. Liu, S.G. Benoit, P.L. Taberna, P. Simon, Understanding of carbon-based supercapacitors ageing mechanisms by electrochemical and analytical methods, J. Power Sources 366 (2017) 123–130.
[49] W.J. Cao, M. Greenleaf, Y.X. Li, D. Adams, M. Hagen, T. Dong, J.P. Zheng, The effect of lithium loadings on anode to the voltage drop during charge and discharge of Li-ion capacitors, J. Power Sources 280 (2015) 600–605.
[50] R. German, P. Venet, A. Sari, O. Briat, J.M. Vinassa, Improved supercapacitor floating ageing interpretation through multipore impedance model parameters evolution, IEEE Trans. Power Electron. 29 (2014) 3669–3678.
[51] J. Vetter, P. Novák, M.R. Wagner, C. Veit, K.C. Möller, J.O. Besenhard, M. Winter, M. Wohlfahrt-Mehrens, C. Vogler, A. Hammouche, Ageing mechanisms in lithium-ion batteries, J. Power Sources 147 (2005) 269–281.
[52] L.A. Middlemiss, A.J.R. Rennie, R. Sayers, A.R. West, Characterisation of batteries by electrochemical impedance spectroscopy, Energy Rep. 6 (2020) 232–241.
[53] X. Zhou, J. Huang, Z.Q. Pan, M.G. Ouyang, Impedance characterization of lithium-ion batteries aging under high temperature cycling: importance of electrolyte-phase diffusion, J. Power Sources 426 (2019) 216–222.
[54] K. Karuppasamy, D. Vikraman, J.H. Choi, R. Bose, A. Nichelson, T. Maiyalagan, H. S. Kim, Hybrid lithium-ion capacitors based on novel 1-butyl-3-methylimidazolium bis (nonafluorobutanesulfony1 imide) (BMImBNFSI) ionic liquid electrolytes: a detailed investigation of electrochemical and cycling behaviors, J. Mater. Res. Technol. 9 (2020) 5216–5227.